Analysis of an E-Core Interior Permanent Magnet Linear Oscillating Actuator

Z. Q. Zhu, *Fellow, IEEE*, and X. Chen

Department of Electronic and Electrical Engineering, University of Sheffield, Sheffield S1 3JD, U.K.

This paper presents the design, analysis and experimental validation of a single-phase tubular E-core interior permanent magnet (IPM) linear oscillating actuator (LOA). Firstly, the topology is described and its electromagnetic performance, in terms of the air-gap flux density, flux-linkage, back-emf coefficient and thrust force-displacement characteristic, is analyzed by finite element analyses. It shows that it is simple to manufacture compared to E-core SPM actuators and solves the problem of significant leakage flux in C-core actuators. In addition, the E-core IPM actuator is capable of producing reluctance force due to the salient mover structure, which enhances the spring stiffness and is conducive to the oscillation, although has no contribution to the output power. The influence of the magnet pole ratio and split ratio on the performance of the IPM LOA is investigated, and the optimal parameters have been identified with reference to the peak value and flatness of the excitation force-displacement characteristic. Finally, the predicted thrust force characteristics are validated by measurements on a prototype actuator.

***Index Terms*—Actuator, interior magnet, linear motor, oscillating, permanent magnet, tubular motor.**

I. Introduction

RECENTLY, single-phase permanent magnet (PM) linear oscillating actuators (LOAs) become increasingly popular in many industrial applications, such as compressors, pumps, vibrators, etc. [1]–[6], mainly because of their inherent high power density and high efficiency. In [6] a planar flux concentration type IPM LOA was proposed, and its performance further was further analyzed in [7]. While due to the advance of soft magnetic composite material [8] proposed a tubular quasi-Halbach magnetized PM LOA, the performance of machines equipped with non-magnetic and ferromagnetic mover back-iron was compared, the efficiency of $>93\%$ being recorded for both cases. In [9] alternative actuator topologies were described, and their finite element (FE) predicted electromagnetic performance was compared. Consequently, a 3-pole interior PM (IPM) topology was identified and further analyzed in [10]. However, the investigation in [8]–[10] only focused on the C-core PM actuators.

In contrast, [11] presented alternative design concepts of single-phase tubular moving-magnet LOAs, both C-core and E-core, and concluded that the preferred stator tooth number N_t and the mover pole number N_p were defined by $|N_t - N_p| = 1$. In addition, a 2-pole, E-core tubular LOA equipped with Halbach surface-mounted permanent magnets (HSPM) was also studied and significant performance improvement was achieved, compared to the actuator with radially magnetized surface PM (SPM) mover.

In this paper, an E-core IPM actuator based on [11] is proposed, which, unlike the SPM and HSPM LOAs having complex mover structures, the mover in the IPM actuator is very simple and easy to manufacture. It also solves the problem of significant leakage flux in C-core actuators. The electromagnetic performance of the LOA is analyzed, and its key design parameters, i.e., the magnet pole ratio and the split ratio, are optimized. Finally, the predicted thrust force characteristics of the E-core IPM LOA are compared with measurements on a prototype actuator.

Manuscript received March 05, 2009. Current version published September 18, 2009. Corresponding author: Z. Q. Zhu (e-mail: Z.Q.Zhu@sheffield.ac.uk).

Color versions of one or more of the figures in this paper are available online at http://ieeexplore.ieee.org.

Digital Object Identifier 10.1109/TMAG.2009.2022049

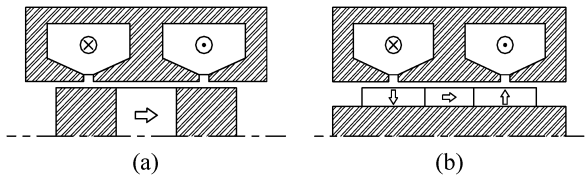

Fig. 1. Schematics of E-core moving-magnet LOAs. (a) IPM. (b) HSPM.

TABLE I
MAIN SPECIFICATIONS OF E-CORE IPM LOA

Items	Analyzed	Prototype
Axial length, L_a	40 mm	44 mm
Stator outer radius, R_o	32 mm	
Stator bore radius, R_s	12 mm	17 mm
Mover shaft radius, R_r	-	3 mm
Air-gap length, g	1 mm	
Stator slot pitch, τ_s	20 mm	
Mover pole pitch, τ_p	20 mm	
Axial length of iron pole, τ_{Fe}	10 mm	12 mm
Axial length of PM ring, τ_{pm}	10 mm	8 mm
NdFeB magnet remanence, B_r	1.2 T	
Rated stroke, A_R	±5 mm	

II. Machine Topology

Fig. 1(a) shows the cross-section of the proposed E-core IPM actuator. The stator is formed by an E-shaped ferromagnetic stator core and two annular coils connected in series and carrying currents which flow in opposite directions, whilst the mover is composed of an axially magnetized PM ring sandwiched between two iron pole-pieces. Compared to the HSPM LOA described in [11] and shown in Fig. 1(b), this actuator has an essentially identical stator structure, but a much simpler mover. Mild steel is employed as the ferromagnetic core, together with NdFeB magnet. The main specifications of the IPM LOA are given in Table I.

0018-9464/$26.00 © 2009 IEEE

Authorized licensed use limited to: Santa Clara University. Downloaded on February 9, 2010 at 02:11 from IEEE Xplore. Restrictions apply.

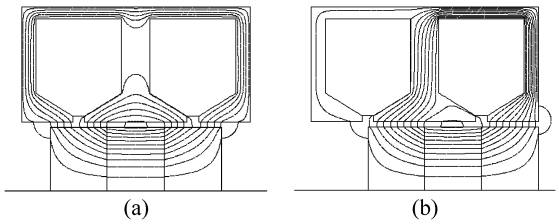

Fig. 2. Open-circuit field distributions of E-core IPM LOA. (a) $Z_d = 0$ mm. (b) $Z_d = +5$ mm.

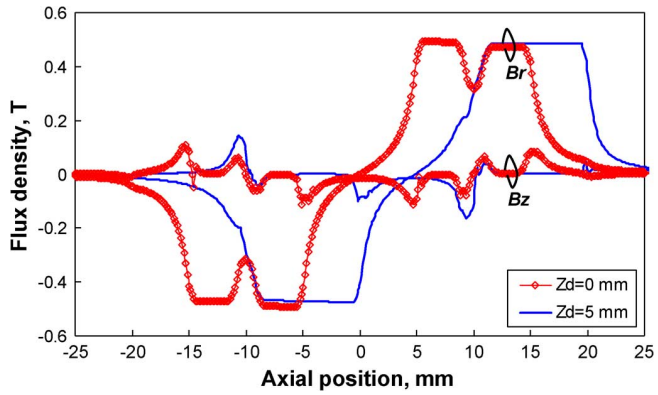

Fig. 3. Open-circuit air-gap field distributions ($r = 11.5$ mm).

III. Analysis of E-Core IPM LOA

Fig. 2 shows the finite element predicted open-circuit field distributions when the mover is at the central rest and displacement $(Z_d) = +5$ mm positions, respectively, and their corresponding air-gap flux density distributions are shown in Fig. 3, in which the waveforms of $Z_d = +5$ mm are essentially shifted from that of $Z_d = 0$ mm, the discrepancies are mainly due to the slotting effect.

The predicted force-mover displacement characteristics are shown in Fig. 4. As can be seen, although the magnitude of cogging force is relatively small, the central rest point is a stable position due to the negative stiffness of cogging force being -356.4 N/m. The total thrust force and reluctance force are respectively calculated with and without permanent magnets, when the actuator is excited with DC current $(J = 3$ A/mm$^2)$. The significant reluctance force is mainly caused by the variation of the winding inductance over the stroke range, Fig. 5. However, it is also evident that the reluctance force, similar to cogging force, will not contribute the output power during operation but will enhance the spring stiffness with its equivalent value being -5149 N/m under DC excitation and -1287 N/m under AC operation with the peak value of sinusoidal current equal to the DC current. The excitation force, produced by the interaction of permanent magnets and the current and the only force component contributing to the power output, is obtained by deducting the cogging and reluctance components from the total thrust force, which maintains a rather flat profile over the range of ± 3 mm at 45 N, but rolls off to 30 N at ± 5 mm, mainly due to the fringing flux at the axial ends of the iron pole-pieces, Fig. 3. The average of thrust force over the rated stroke, ± 5 mm, is $\sim$42 N. The flux-linkage characteristic varies almost linearly as the mover is displaced from the centre but becomes slightly saturated as it approaches the ends of stroke, Fig. 6. Thus, the back-emf coefficient, K_E, defined as the derivative of

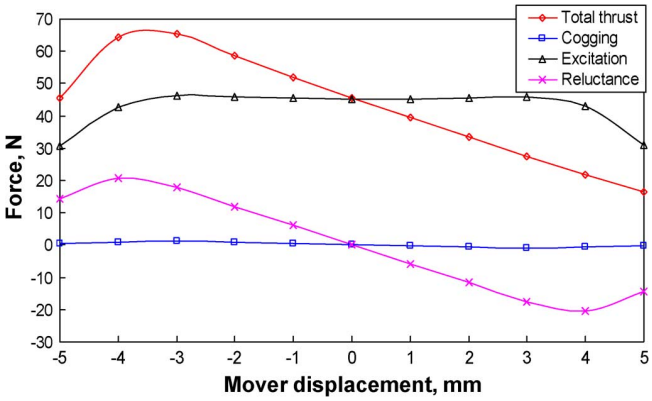

Fig. 4. FE predicted thrust force-mover displacement characteristics.

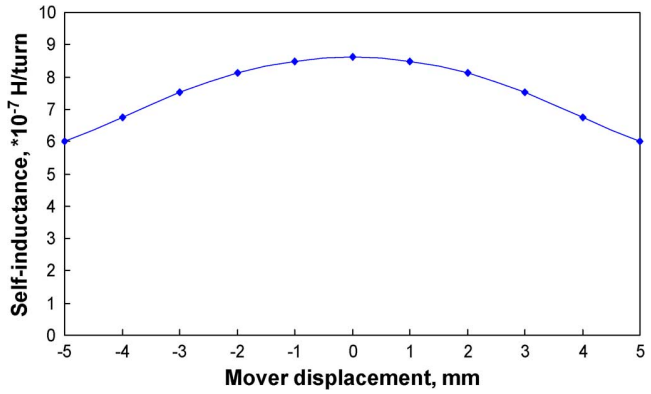

Fig. 5. Variation of winding inductance with mover displacement.

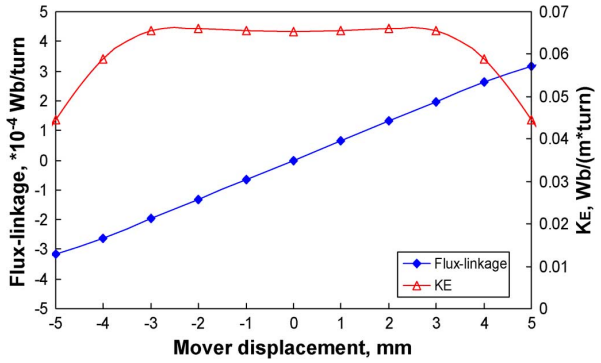

Fig. 6. Variations of flux-linkage and back-emf coefficient with mover displacement.

flux-linkage over mover displacement, is also shown in Fig. 6, and, as expected, exhibits essentially identical profile as the excitation force, Fig. 4, having an average of $\sim$0.061 Wb/m.

IV. Design Optimization

The magnet pole ratio, $\alpha_p = \tau_{Fe}/(\tau_{Fe} + \tau_{pm})$, and the actuator split ratio, $\alpha_s = R_s/R_o$, greatly influence the specific thrust force capability of the LOA. Thus, α_p and α_s have been optimized with reference to the LOA studied earlier, by fixing the actuator outer radius, the copper loss, the stator tooth width, the stator back-iron thickness, the stator slot opening, the actuator axial length, the slot- and pole-pitches. Based on the sinusoidal current control, it is assumed the mover velocity is also sinusoidal and in-phase with the current due to the mechanical low-pass filter effect. The maximum excitation force will occur

Authorized licensed use limited to: Santa Clara University. Downloaded on February 9, 2010 at 02:11 from IEEE Xplore. Restrictions apply.

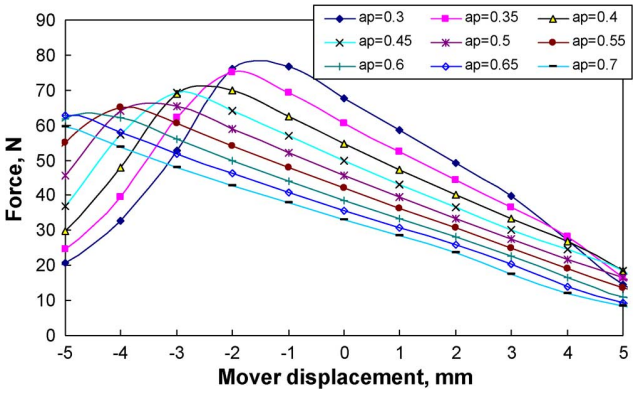

Fig. 7. Variations of force with mover displacement at different α_p when $\alpha_s = 0.375$ and $p_{Cu} = 5$ W.

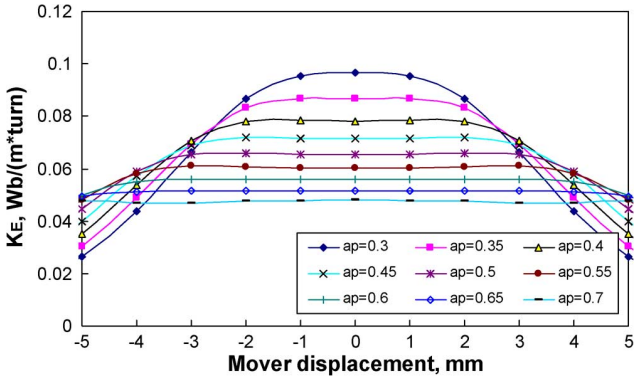

Fig. 8. K_E-mover displacement characteristics ($\alpha_s = 0.375$).

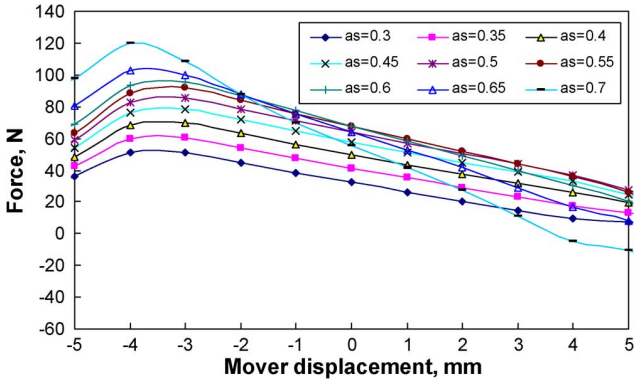

Fig. 9. Variations of force with mover displacement at different α_s when $\alpha_p = 0.5$ and $p_{Cu} = 5$ W.

at the central position. Therefore, the aim of the optimization is to find a good balance between the maximum value at 0 position and the flatness of the excitation force.

Fig. 7 shows the various force-mover displacement characteristics predicted by FE analyses, when α_p varies between 0.3 and 0.7 but $\alpha_s = 0.375$ and fixed copper loss ($p_{Cu} = 5$ W). It is evident that the slope and peak force increase as α_p decreases. Since the excitation force is critical to the production of output power during operation, it is worth to be studied further. However, because of the difficulty to separate the excitation and reluctance forces especially in saturated scenarios, the K_E-mover displacement characteristic, Fig. 8, is used to indicate the influence of α_p on the excitation force. As can be seen, both the peak value and the non-linearity of K_E become more significant with

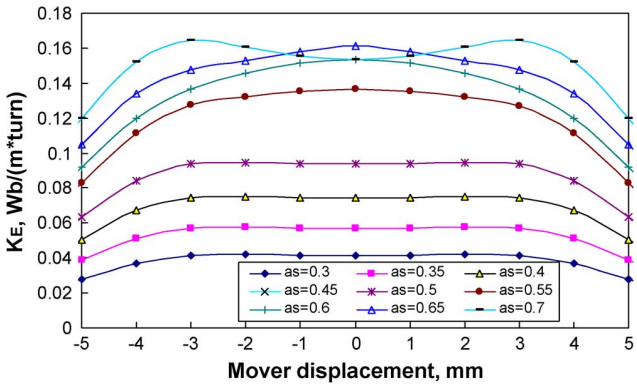

Fig. 10. K_E-mover displacement characteristics ($\alpha_p = 0.5$).

smaller α_p, mainly due to the enhanced air-gap flux density but shortened axial pole length.

Fig. 9 shows the variation of the thrust force with α_s when $\alpha_p = 0.5$ and $p_{Cu} = 5$ W, whilst Fig. 10 shows the K_E-mover displacement characteristics with different α_s. It can be seen that both the slope and peak force increase as α_s increases due to the increase of air-gap flux density and the increase of cogging force, respectively. Similarly, the peak value and the non-linearity of K_E increase as α_s increases. Compared to the rest, the different curve profile with $\alpha_s = 0.7$ is mainly caused by the magnetic saturation in the stator back-iron.

Based on the foregoing analyses, the optimal actuator design should exhibit big peak K_E/excitation force and rather flat profiles over the rated stroke. Hence, the global optimization with regard to α_p and α_s is undertaken by calculating two parameters:

$$F(0) = F(Z_d = 0) \tag{1}$$

$$\varsigma = \max\left(\frac{|K_E(Z_d) - K_E(0)|}{K_E(0)}\right) \tag{2}$$

where $F(0)$, used as the approximation of peak excitation force, is the thrust force at the central position with current injections, as both the cogging and reluctance forces are ~0, whilst ς is employed as an index for the non-linearity of K_E-displacement characteristics. Fig. 11 shows the variation of the magnet pole ratio and split ratio on the FE predicted $F(0)$ and ς, when α_p and α_s both being varied from 0.3 to 0.7. It can be seen that the optimal α_s is essentially identical, ~0.58, irrespective of α_p changes, and for specific α_p the variation of ς is insignificant especially when α_s is small. When combining the two parameters, Fig. 12 indicates that the combination of $\alpha_p = 0.6$ and $\alpha_s = 0.5$ is close to the optimal.

V. Comparison With Measurements

In order to validate the foregoing FE analyses, a prototype actuator, Fig. 13(a), has been designed, with the resonant frequency = 50 Hz, the output power = 42 W and the predicted efficiency = 89%. The total and moving masses are 866 g and 230 g, respectively. However, for the consideration of application dimensions of the fabricated prototype are slightly different from those used in the foregoing analyses, as highlighted in Table I. Further, in order to enhance the mover integrity the magnet and mild steel are made of rings, rather than solid disks, mounted on a shaft of 3 mm radius, as can

Authorized licensed use limited to: Santa Clara University. Downloaded on February 9, 2010 at 02:11 from IEEE Xplore. Restrictions apply.

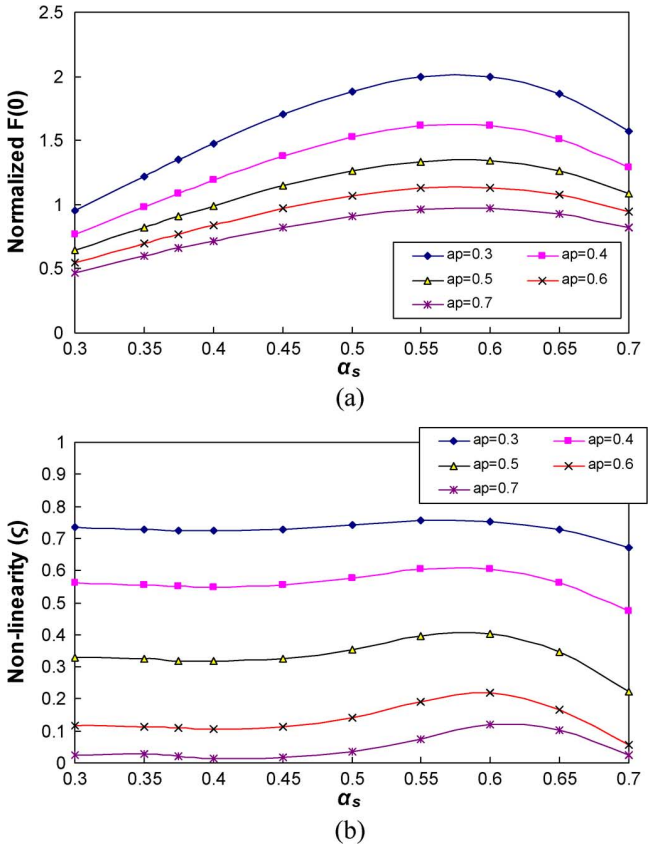

Fig. 11. Variations of the FE predicted $F(0)$ and ς. (a) $F(0)$; (b) ς.

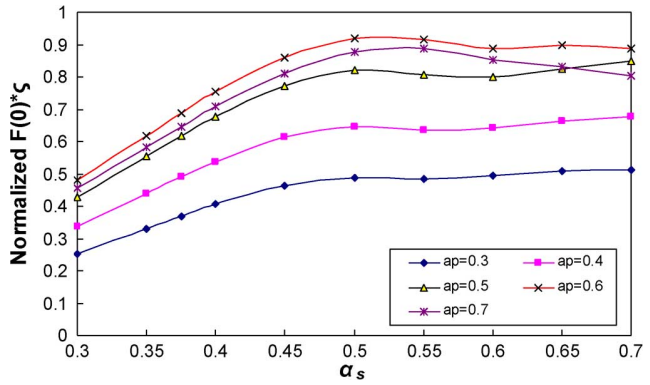

Fig. 12. Variation of $F(0)$*ς.

be seen in Fig. 13(a). Fig. 13(b) shows the static test bench used to measure the cogging force and static thrust force-mover displacement characteristics. As can be seen in Fig. 14, good agreement between the measured and corresponding FE predicted results is achieved.

VI. Conclusion

A tubular E-core IPM linear oscillating actuator has been designed and its electromagnetic performance, in terms of the air-gap flux density, flux-linkage, back-emf coefficient and thrust force-displacement characteristic is analyzed by finite element analyses. It shows that the E-core IPM actuator yields a reluctance force due to the salient mover structure, which enhances the spring stiffness and is conducive to the oscillation, although has no contribution to the output power. The influence

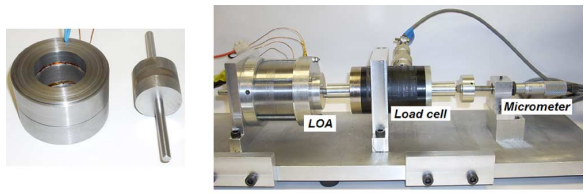

Fig. 13. Prototype actuator and static test bench. (a) Prototype stator and mover. (b) Test bench.

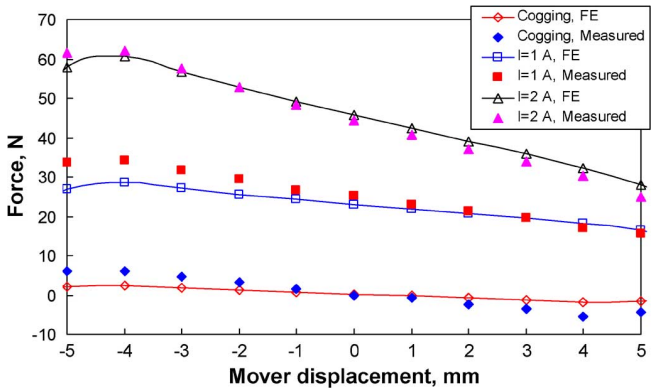

Fig. 14. Comparison of predicted and measured thrust force-mover displacement characteristics.

of the magnet pole ratio and split ratio on the performance of the IPM LOA is investigated, and the optimal parameters have been identified with reference to the peak value and flatness of the excitation force-displacement characteristic. Finally, the predicted thrust force characteristics are validated by measurements on a prototype actuator.

Acknowledgment

This work was supported by the Engineering and Physical Sciences Research Council, UK, Ref. EP/E01190X.

References

[1] I. Boldea and S. A. Nasar, *IEEE Trans. Energy Conversion*, vol. 14, no. 3, pp. 712–717, 1999.
[2] R. Redlich, "A Summary of Twenty Years Experience With Linear Motors and Alternators," Sunpower Inc., 1995 [Online]. Available: http://www.sunpower.com/
[3] K. B. Park, E. P. Hong, and H. K. Lee, "Development of a linear motor for compressors of household refrigerators," in *Proc. 3rd Int. Symp. Linear Drives for Industry*, Japan, 2001, pp. 283–286.
[4] M. Watada, K. Yanashima, Y. Oishi, and D. Ebihara, *IEEE Trans. Magn.*, vol. 29, no. 6, pp. 3361–3363, 1993.
[5] T. Mizuno, Y. Bu, M. Ohkubo, F. Tsuchiya, and H. Yamada, "Static thrust analysis of a moving magnet linear oscillatory actuator for vibration cancel system," in *Proc. 5th Int. Symp. Linear Drives for Industry Applications*, Japan, 2005, pp. 282–285.
[6] T. H. Kim, H. W. Lee, Y. H. Kim, J. Lee, and I. Boldea, *IEEE Trans. Magn.*, vol. 40, no. 4, pp. 2092–2094, 2004.
[7] L. Tutelea, M. Kim, M. Topor, J. Lee, and I. Boldea, *IEEE Trans. Ind. Electron.*, vol. 55, no. 2, pp. 492–500, 2008.
[8] T. Ibrahim, J. Wang, and D. Howe, *IEEE Trans. Magn.*, vol. 44, no. 11, pp. 4361–4364, 2004.
[9] A. G. Jack, Z. S. Al-Otaibi, and M. Persson, "Alternative designs for oscillating linear single phase permanent magnet motors using soft magnetic composites," presented at the 2006 Int. Conf. Electrical Machines and Systems, Japan, 2006, Paper ID. DS4F2-07.
[10] Z. S. Al-Otaibi and A. G. Jack, in *Proc. 2006 Universities Power Engineering Conf.*, 2006, pp. 705–708.
[11] Z. Q. Zhu, X. Chen, D. Howe, and S. Iwasaki, *IEEE Trans. Magn.*, vol. 44, no. 11, pp. 3855–3858, 2008.

Authorized licensed use limited to: Santa Clara University. Downloaded on February 9, 2010 at 02:11 from IEEE Xplore. Restrictions apply.